RESEARCH ARTICLE   OPEN ACCESS

Comparative Study and Evaluation of Two Different Finite Element Models for Piston Design

H. Adil[1], S. Gerguri[1],J. Durodola[1],N. Fellows[1], F. Bonatesta[1], F. Audebert[1,2,3]

[1] *School of Engineering, Computing and Mathematics, Oxford Brookes University, Wheatley Campus, OX33 1HX, Oxford, United Kingdom*
[2] *Grupo de Materiales Avanzados, INTECIN (UBA-CONICET), Facultad de Ingeniería, Universidad de Buenos Aires. Paseo Colón 850, Ciudad de Buenos Aires (1063), Argentina.gma@fi.uba.ar*
[3] *Department of Materials, University of Oxford, 16 Parks Road, OX1 3PH, Oxford, United Kingdom*
Corresponding Author: H. Adil

ABSTRACT
The exposure of pistons to extreme mechanical and thermal loads in modern combustion engines has necessitated the use of efficient and detailed analysis methods to facilitate their design. The finite element analysis has become a standard design optimisation tool for this purpose. In literature two different approaches have been suggested for reducing the geometry of the cylinder and crank slider mechanism,toidealise piston finite element analysisload models,whilst trying to maintain realistic boundaries to obtain accurate results. The most widely used geometry is the combination of piston and gudgeon pin while the second geometry includes some portion of the connecting rod's small end and cylinder in addition to the piston and gudgeon pin.No clear analyses have been made in literature about the relative effectiveness of the two approaches in terms ofmodel accuracy. In this work both approaches have been carried out and analysed with respect to a racing piston. The results suggest that the latter approach is more representative of the load conditions that the piston is subjected to in reality.
Keywords: Ansys, Finite Element Analysis, Piston, Stress

I. INTRODUCTION

Pistons are critical components inpower conversion systems in engines as they transfer energy from the combustion of the air-fuel mixture to the crankshafts through the connecting rods. An engine power system consists of a crank-train, a piston, agudgeonpin and a connecting rod [1].Pistons are also one of the most stressed moving components due to the combustion gases [2]. They must be designed to withstand the thermal and dynamic loads and avoid structural failure, noise and skirt scuffing. They should also be light enough to minimise inertial loads, reduce friction and transmit heatgeneration [1-2].

The increasing performance requirements of modern combustion engines have exposedpistons to extreme loads and temperatures. Therefore, the use of physically based and efficient calculation methods is critical for the prediction of structural integrity and reliability. The finite element analysis (FEA) method has become awell-accepted procedure in the industry to make predictions before expensive manufacturing and testing are carried out [3].The formulation of a finite element (FE) model for piston requires the computer aided design (CAD) geometries of the piston and other relevant components. Two different approaches are used in literaturefor the idealisation of the piston FEA load models; of which the most widely used simplification being the use ofpiston and gudgeon pingeometry only [4-6]. Mahle[3]suggests that the geometry used for a piston FEA should includesome portion of the connecting rod's small end and a cylinder in addition to the piston and gudgeon pin. The aim of this paper is therefore to analyseboth approaches to select a geometry that is more representative of the piston's actual operational conditions.The piston used in this work is fromamotorbike engine and it was reversed engineered using a laser scanning technique. The load calculations require some engine parameters, which are given in Table 1.

Engine Type	KTM Single cylinder, 4-stroke
Total Displacement/Volume (V_t)	449.30 cc
Bore (B)	97 mm
Stroke (S)	60.8 mm
Compression Ratio (r_c)	12.5:1
Connecting Rod Length (l)	107.40 mm

Table 1. The engine specification for a KTM 450 XC-F 2008.

1.1 Methodological Approach

The methodology for the undertaken work is divided into twosections (see sections II and III). The first section discusses the two different CAD geometries and constraint conditions used in the different modelling approaches. The second section involvesthe determination of the different engine loads actingon the pistonduring engine operation and how these loads are implemented in the FEA. In general, the paper presents details of the thermo-mechanical loads and boundary conditions that should be included in carrying out the finite element analysis of a piston for an internal combustion engine. It also includes the incorporation of contact analysis that is essential for the modelling of interaction of parts in model assemblies.

II. CAD GEOMETRIES AND CONSTRAINTS FORFINITE ELEMENT ANALYSIS (FEA)

Idealisation of the geometry is a common practice in formulating finite element (FE) models to enable rapid meshing, reduced processing time and reduced resource requirements. Given that real-world loading and constraint conditions can be represented, the reduced geometry model is considered to be an adequate representation of the actual structure. Eliminating certain parts and features may remove interdependencies that could lead to flawed results.

For a piston finite element analysis (FEA), most of the published papers include a piston and gudgeon pin in the geometry (shown asmodel1 in Fig. 1). However, Mahle[3]suggests including some portion of the connecting rod's small end and a cylinder in addition to the piston and gudgeon pin (shown asmodel 2in Fig. 2). Mahle[3] does not explain whymodel 2 is better than model 1, but states that there are three types of mechanical loads acting on a piston including lateral force, which most of the published papersdo not account for. In this work, equations have been derived from the crank slider mechanism [7] to calculatethe lateral force (see section 3.1.3) for inclusionin the FEA to evaluate its effect on the piston deformations. According to the dynamic and free body diagram analysis of the crank slider mechanism, nearly one-third of the connecting rod's mass acts on the piston side of the crank slider mechanism[7]. The inertia force acts in the opposing direction to the effect of the combustion pressure [8].

For model 1 of the piston FEA the pin-connecting-rod interfacewas constrained using a cylindrical support as suggested by[4]. This constraint willprevent realistic deformation of the pin and also prevent the transfer of the forces fully onto the piston, especially the lateral force. In reality the pin is supported by the connecting rod. The unrealistic deformation of the pin when using the cylindrical support will affectthe piston deformations as well; the results obtained in this work supported this hypothesis too. Furthermore, model 1 does not allow preventing the rotating motion of the piston around the piston pin axis.

To constrain model 2; a node was fixed in the middle of theconnecting rod's bottom face andfixed supports were used on the bottom cylinder washers and studs to represent the cylinder being attached to the engine body. Furthermore, a pressure of 5.22 MPa was applied to the top washers to represent the clamping force of 30 Nm that is applied to the studs/nuts on the cylinder.The contacts between piston-pin,pin-connecting-rod and piston-cylinder were specified as frictional contacts which requiredthe friction coefficient values to be specified. Using contacts to define the interactions between the different components should give results close to reality[3] if appropriate friction coefficients are used. Determining the real friction coefficient values between these contactsthough is practically difficult. Other researchers such as [9] have tried to determine these coefficients, giving values that change with the engine speed. A constant value of 0.01, used in this work, is however generally used[4].
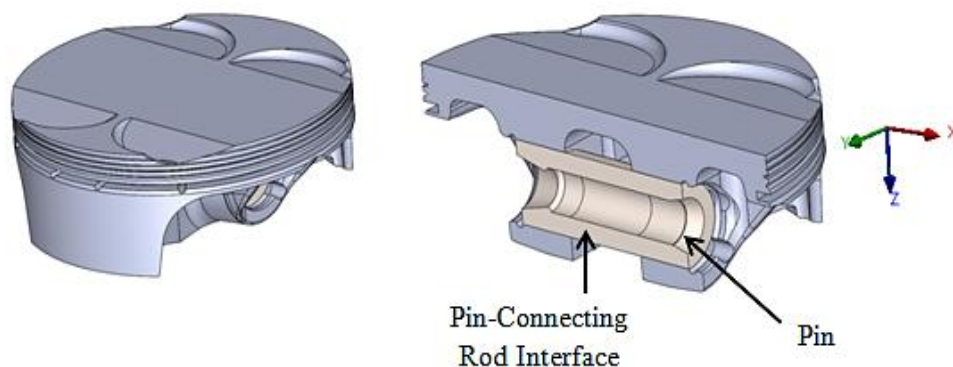
Figure 1. Model 1 assembly for piston FEA.
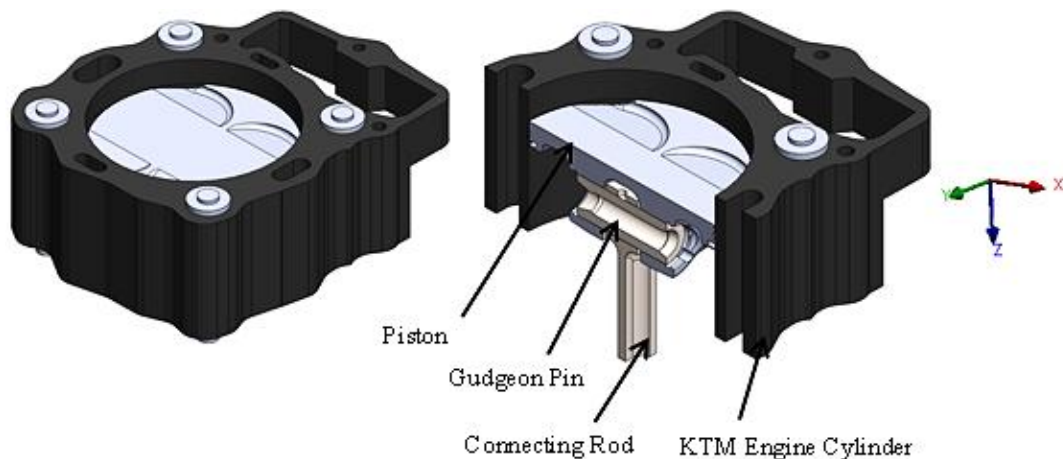
Figure 2. Model 2 assembly for piston FEA.

The aluminium alloy used forthe engine's piston is 4032-T6 and its mechanical properties are given in Table 2 [10-11].

Property	Value
Density (Kg/m^3)	2690
Elastic Modulus (GPa)	79
Poisson Ratio	0.33
Thermal Conductivity (W/mK)	155 at 25 °C
Thermal Expansion (1/°C)or (µm/m°C)	19.4×10^{-6}
Yield Strength (MPa)	331 at 25 °C
	300 at 100 °C
	62 at 200 °C
	24 at 300 °C

Table 2. Mechanical properties of the Al 4032-T6 [10-11].

III. DETERMINATION OF THE ENGINE LOADS ON PISTON

There are mechanical and thermal loads acting on an engine piston during operation. These operating loads are affected by the type of engine (such as two, four stroke, diesel etc) and the design of the engine. The mechanical and thermal loads are presentedseparately in sections 3.1 and 3.2. These loads are then applied to the model, in section 3.3, at critical points in terms of piston failure, due to the piston stresses, within an engine cycle.

3.1 Mechanical Loads

Three different mechanical loads act on a piston, which are the combustion pressure and the inertial and lateral forces. The different loads and the crank slider mechanism are depicted in Fig. 3. The different mechanical forces are considered in sections 3.1.1, 3.1.2 and 3.1.3.
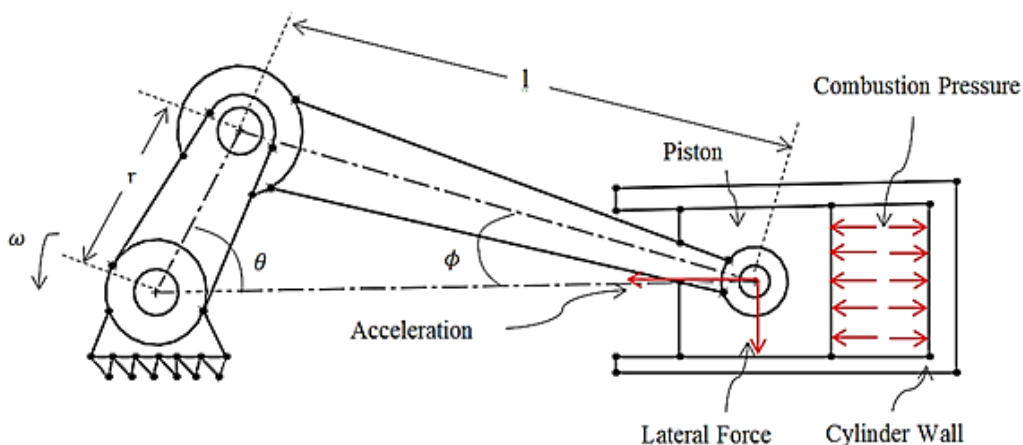
Figure 3.A representation of the crank slider mechanism and the piston mechanical loads.

3.1.1 Combustion pressure

The combustion gas pressure of the air-fuel mixture on the piston was modelled as a pressure acting on the piston's crown and wasapplied over the entire piston's crown going down to the lower flank of the compression ring grooveas suggested in reference [3]. The engine used in this work, see Table 1, was tested in reference [12] giving the pressure cycle shown in Fig. 4. This pressure cycle has been used in this work to define the pressure acting on the piston crown.
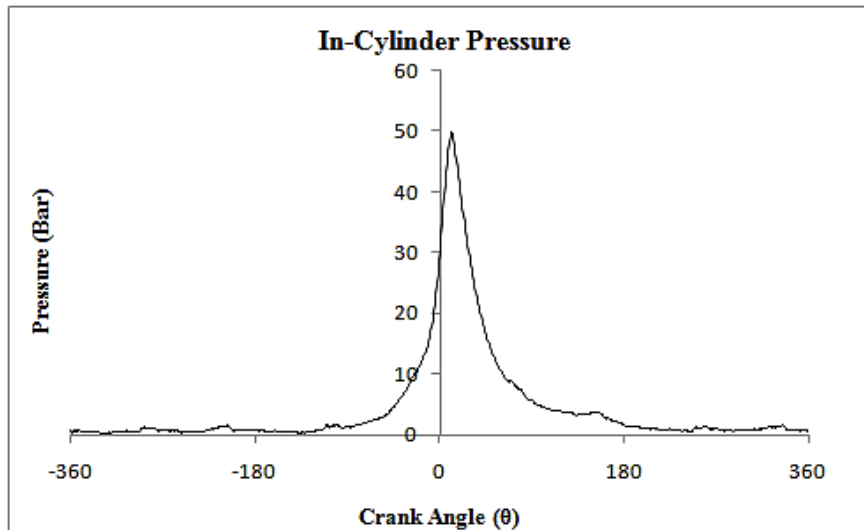
Figure 4. Pressure trace for theKTM test engine at 7000 rpm [12].

3.1.2 Inertial force/ acceleration

The oscillating motion of a piston in a cylinder produces accelerations that reach their maximums at the cylinder's dead centres. The acceleration was applied globally to the FE modelas suggested in references[3] and [13]and was determined from equation (1) [7,14]. Piston accelerations for the test engine over one engine cycle are plotted in Fig. 5.

$$\ddot{x} = -r\omega^2(\cos\theta + \frac{r}{l}\cos 2\theta)$$

(1)

where $\ddot{x}, r, \omega, \theta$ and l are the piston's acceleration, crank offset or crank radius, crank angular velocity, crank angle and the connecting rod length respectively.

The crank radius (r) is the distance between the crank pin and crank centre or half of the stroke.The crank angular velocity is related to the engine speed (N) in revolution per minute (RPM) by equation (2)

$$\omega = 2\pi N/60 \qquad (2)$$
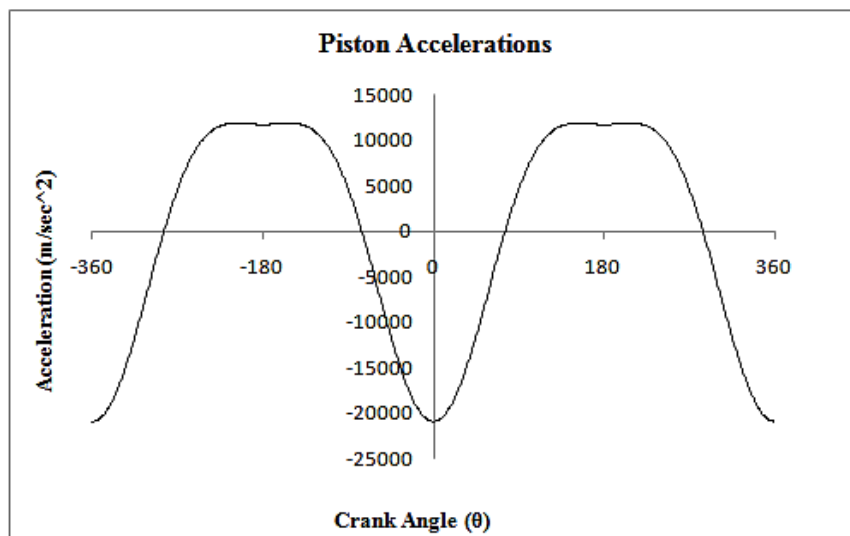
Figure 5. Piston accelerations for the test engine over one engine cycle at 7000 rpm.

3.1.3 Lateral force

The conversion of a piston's linear motion into the crankshaft's rotational motion generates force components in the crank mechanism that presses the piston against the cylinder wall as illustrated in Fig. 3. In the FE modelling, the lateral force (L_f) is transmitted into the piston throughthe pin and connecting rod [3]. In the case of model 2, the lateral force was applied on the face of the connecting rod that is in contact with the pin (in the pin end bore), while for model 1, the lateral force was applied on the pin-connecting rod interface.

The lateral force is made up of the gas pressure forceand the inertial force and can be determined using equation(3) [7].

$$L_f(\theta) = -(m_B \ddot{x} + F_g) \tan\phi \qquad (3)$$

Wherem_B is the mass of the reciprocating components that include the piston, the pin and approximately one-third of the connecting rod's mass. $\Phi$is the angle that the connecting rod makes with the cylinder axis (Fig. 3) and can be determined from equation (4) [7].

$$\sin\phi = \frac{r}{l} \sin\theta \qquad (4)$$

$F_g$is the gas force and can be calculated from equation (5) [7].

$$F_g(\theta) = -\frac{\pi}{4} B^2 P(\theta) \qquad (5)$$

where B and P arethe engine's bore and the gas pressure respectively.

The lateral force for the test engine over one engine cycle based on equation (3) is shown in Fig. 6.
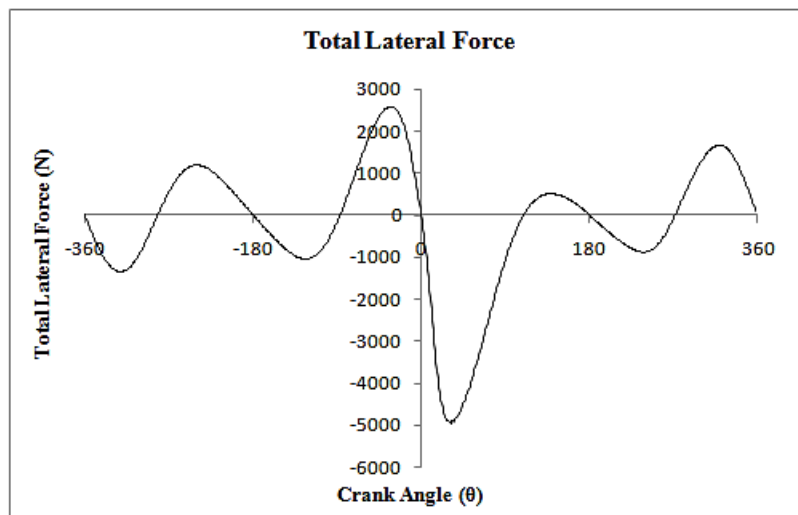
Figure 6. Total lateral force during thetestengine cycle at 7000 rpm.

3.2 Thermal Loads

The thermal load from the combustion of theair-fuel is also a cyclic load on the piston. It acts mainly during the expansion stroke on the combustion side of the piston. The thermal load has a very high peak at the point of combustion, but the duration of this peak is very short (only a few milliseconds depending on the engine speed). This peak generates a cyclic loading on the piston crown, but this temperature fluctuation only occurs close to the surface of the material within the piston, which is exposed to the combustion gases. Most of the pistonmass reaches a quasi-static temperature during engine operation with limited cycle variation. Although there is no cycle variation there is still significant variation of the quasi-static temperature within the piston. The heat transfer from the combustion gas to the piston takes place predominantly by forced convection, and only a small portion by radiation [3].

In the thermal FE analysis of the piston; the quasi-static temperature was modelled using steady state conditions. The heat transfer calculationsrequirethe determination ofthe combustion gas temperature. The gas temperature in the cylinder varies considerably depending onthe state of the combustion. As an approximation,the ideal gas law described by equation (6)was used to determine the mean gas temperature indirectly from the in-cylinder pressure [15].

$$T(\theta) = \frac{P(\theta)V(\theta)}{nR} \qquad (6)$$

where P, V, n, R and T are the in-cylinder pressure, cylinder volume, combustion product in moles, universal or ideal gas constant and the gas temperature respectively. The momentary cylinder volume can be calculated using equation(7) [16].

$$V(\theta) = V_c + \left(\frac{\pi B^2}{4}\right)(l + r - x) \qquad (7)$$

WhereV_c and x are the clearance volume and the piston position respectively. The clearance volume can be obtained using equation(8) [16].

$$V_c = \frac{V_t}{(r_c - 1)} \qquad (8)$$

WhereV_t is the engine's total volume and r_c is the compression ratio. The value of$x$in equation (7) in terms of the angular position (θ) can be determined using equation (9).

$$x = l - \frac{r^2}{4l} + r\left(\cos\theta + \frac{r}{4l}\cos 2\theta\right)$$
(9)

The product or mass of the combustion in moles can be calculated using (10).

$$n = m/M \qquad (10)$$

where m and M are mass of the fuel or the air in grams and molar mass of the fuel or the air in g/mol respectively.

Having used equations 6-10 to determine the combustion gas temperature the heat transfer between the piston and its surroundings can be evaluated. Sections 3.2.1 to 3.2.5 explore the different areas of the piston where the heat transfer takes place.

3.2.1 Heat transfer between the combustion gas and piston crown

The heat transfer coefficient (HTC) of the hot gases can be obtained from one-dimensional thermodynamic analysis of theengine cycle. There are numerous models that have been put forward to determine the heat transfer coefficient of these gases inside the cylinder. The Hohenbergmodel described by equation (11) [15] wasused to determine the instantaneous heat transfer coefficient of the hot gases. The Hohenbergmodel was based on extensive experimental observations, which was obtained after detailed examination of the Woschni's model [17-18].

$$h(\theta) = C_1 V(\theta)^{-0.06} P(\theta)^{0.8} T(\theta)^{-0.4} (V_p + C_2)^{0.8}$$
(11)

where h, P and V_p are the heat transfer coefficient (W/m^2K) of the hot gases, cylinder pressure (bar) and the piston mean speed (m/sec) respectively. C_1andC_2 are constants and their mean values are 130 and 1.4 respectively. The piston's mean speed can be determined using equation (12) [16].

$$V_p = 2SN \qquad (12)$$

where S and N are engine stroke (m) and engine speed (rpm) respectively.

Forthe steady state thermal analysis considered here, the mean heat transfer coefficient (h_m) and the mean gas temperature (T_m) values were used. These can be obtained using equations(13) and (14) [19].

$$h_m = \frac{1}{720} \int_0^{720} h(\theta)\ d(\theta)$$
(13)

$$T_m = \frac{1}{720 \times h_m} \int_0^{720} h(\theta) T(\theta)\ d(\theta)$$
(14)

The hot gases heat transfer coefficient was applied to the entire piston's crown and down up to the compression ring groove in both models. However in model 2, the same HTC was also applied to the inside of the cylinder over the area of the cylinder that was above the piston crown, as that area is also exposed to the hot gases. The portion of the cylinder exposed to hot gases changes over an engine cycle, but since the analyses carried out in this work are static therefore the motion of the piston with respect to the cylinder is not accounted for.

3.2.2 Heat transfer between Compression Ring and Cylinder

A significant amount of heat from the piston exits through the compressing ring which needs to be accounted for in the thermal modelling of a piston. The heat transfer coefficients are different for the upper and lower faces of the compression ring. Determining the real heat transfer coefficients for compression rings are complicated and beyond the scope of this work.The values used in this work were 885 and 1818(W/m^2K) for upper and lower faces respectively with ambient temperature of 160 °C which were obtained from [20].

In the FE models the upper heat transfer coefficient was applied to the upper face of the compression ring groove and the side face of the compression ring groove which is in contact with the thickness side of the compression ring. The lower heat transfer coefficient was applied to the lower face of the compression ring groove.

3.2.3Heat transfer between ring lands, piston outer skirt and the cooling oil

The movement of the lubrication oil film between the ring lands and the outerskirt through convection can be modelled as a laminar flow between two parallel plates [21]. To get the value ofthe heat transfer coefficient; theNusselt number (Nu) for the laminar flow between two parallel plateswas determined using equation(15) [13,21].

$$Nu = \frac{h D_h}{k_{oil}} = 8.235 \qquad (15)$$

The heat transfer coefficient (h)isgiven by equation (16)

$$h = 8.235 \frac{k_{oil}}{D_h} \qquad (16)$$

wherek_{oil} and D_h arethe thermal conductivity of the oil in (W/m K) and hydraulic diameterin (m)respectively. Hydraulic diameter is determined as a function of the cross-sectional area of the plates per unit depth and the wetted perimeter. It was calculated using equation(17) [13,21].

$$D_h = \frac{4A}{P}; A = 2b; \quad P = 2 \quad D_h = 4b$$
(17)

where A, P and b are the cross-sectional area of the plate per unit depth, the wetted perimeterandthe piston-cylinder gap (the lubricating oil film) respectively. In both models,

the HTC was applied to all the outer areas of the piston below the compression ring. Note that defining the HTC requires the engine oil temperature which depends on many factors and therefore not specified by the manufacturer in the engine manual. However, it was suggested by [22] that the average engine oil temperature for this engine when operating at 7000 rpm can reach 100 °C.

3.2.4. Heat transfer between the piston under-crown and inner walls of the piston skirt and the cooling oil

The piston's under crown has a very complex geometry due to the existence of the ribs andthe pin boss soevaluations of theheat transfer coefficients are difficult. The piston's under crown is cooled by oil sprayed onto the underside of the piston. To model this cooling the piston's inner surface was assumed to be cylindrical, with diameter equal to the outer piston diameter,and the cooling oil moving along the innersurface of the cylinder was assumed to have a velocity equivalent to the mean piston velocity. This assumption is based on the Ditus-Boelter correlation which satisfies the turbulent forced convection heat transfer on a cylindrical surface [21]. The correlation gives the Nusselt numberwhich can be used to determine the heat transfer coefficient. The Ditus-Boelter correlation is described by equation (18) [13, 21].

$$Nu = 0.023 Re^{0.8} Pr^n \qquad (18)$$

The Reynolds's and Nusselt's numbers can be determined using equations (19) and (20).

$$Re = \frac{\rho_{oil}\, U_{oil}\, D_h}{\mu_{oil}} \qquad (19)$$

$$Nu = \frac{h_{oil}\, D_h}{k_{oil}} \qquad (20)$$

Substituting equations (18) and (19) into equation (20) leads to equation (21) which can be used to determine the heat transfer coefficient.

$$h_{oil} = 0.023\, D_h^{-0.2} k_{oil} \left(\frac{\rho_{oil}\, U_{oil}}{\mu_{oil}}\right)^{0.8} Pr^n$$
(21)

where Nu, Pr, Re, ρ_{oil}, U_{oil}, μ_{oil},h_{oil} are Nusselt's number, Prandtl number, Reynolds's number, oil density (Kg/m^3), oil flow speed (m/sec), oil dynamic viscosity (kg/m.sec) and heat transfer coefficient of the oil ($W/m^2 K$) respectively. The value of the index n is 0.4, when the oil is being heated and 0.3 when the oil is being cooled [13].

ThePr number can be determined using equation (22).

$$Pr = \frac{\mu_{oil}\, C_p}{k_{oil}} \qquad (22)$$

WhereC_p is the specific heat value of thecooling oil.

In both models, the HTC was applied to the entire underside of the piston and pin, but in model 2 it was also applied to the connecting rod because heat transfers from the piston also takes place to the connecting rod.

3.2.5. Heat transfer between the engine cylinder and cooling water jacket

The heat transfer coefficient of the combustion engine's cooling jacket has been determined experimentally for different engines and presented in literature. However, for the majority of spark ignition (SI) engines, the average value is 1480 ($W/m^2 K$) [23], which has been used in this work. The average water/coolant temperature was suggested to be 100 °C [22].

3.3 Critical Load Cases

It can be deduced from Fig. 4-6 that the maximum values for different mechanical loads occur at different angular positions of the crankshaft. In order to avoid neglecting any combination of these forces that may be critical, a practical number of appropriately selected points in time were analysed. These includethe points at which the individual mechanical loads reached a maximum. This gave three load cases which werethe points of maximum combustion pressure, maximum inertial and maximum lateral forces. The maximum combustion pressure load case that occurred at a crank angle of 17° after the top dead centre (TDC) for the analysed engine speed of 7000rpm, turned out to be the most critical (had the highest piston stresses). The results presented in this work therefore focus on this load case.The mechanical load values for the maximum combustion pressure load case are given in Table 3 below.

Load	Value
Pressure	49.2 bar
Acceleration	19455m/sec²
Lateral Force	3709 N

Table 3. Mechanical load values in the maximum combustion load case.

As was stated in section 2, the FE model include either the piston and pin (Model 1) or piston, pin, connecting rod's small end and the cylinder (Model 2). In this work both models were analysed and the results are presented in section 4. Furthermore, for model 2 the connecting rod was also titled with respect to the cylinder axis with corresponding titling angle i.e. 17°at the point of maximum pressure in the maximum combustion pressure load case.

IV.   RESULTS

The results presented in this section were based on the critical load condition highlighted in section 3.3. Results are presented for temperature (section 4.1), Von Misesstress (section 4.2), strain (section 4.3), principal stress (section 4.4) and deformation (section 4.5). These aspects are significant factors in piston design analysis. A mesh convergence analysis was also carried out which indicated that the mesh converged at an element size of 3.5 mm. The directional Cartesian axes used for analyses align with the pin longitudinal direction (X), radial to the pin longitudinal direction (Y) and the notional direction of the piston motion (Z), as shown in Fig. 2.

4.1 Temperature Distribution

Thermo-mechanical analysis was carried out on the two models using the mechanical loads and heat transfer coefficients determined in sections 3.1 and 3.2 respectively. The quasi-static temperature distribution of the piston for both FE models can be seen in Fig. 7 while the temperature distribution in the cylinder is given in Fig. 8.
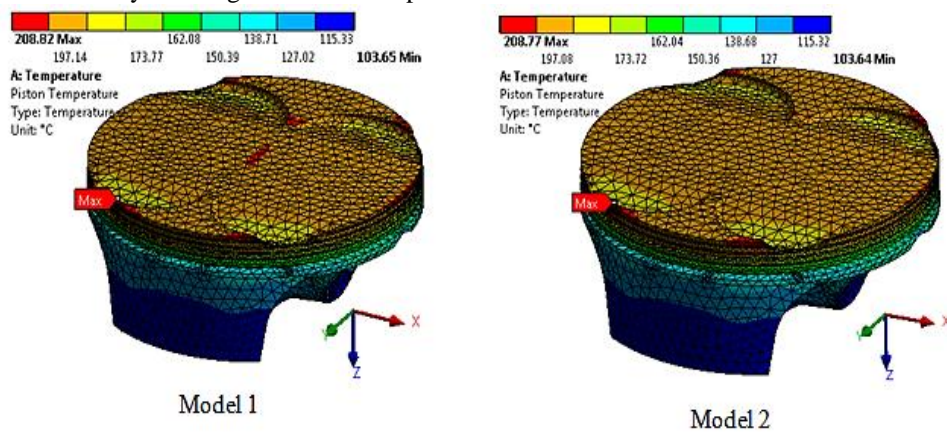
Figure 7. Piston temperaturedistributionsin both FE models.
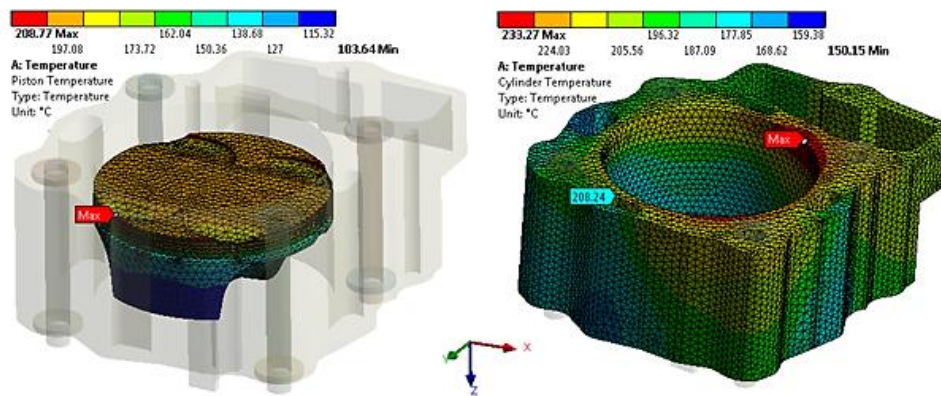
Figure 8. Temperature distribution in cylinder in model 2.

The temperature distribution results showed that the maximum temperature in both FE models is nearly the same and occurred at the locations (valve pocket edges) that were the furthest from any cooling surfaces. However, the temperature distribution in model 1 is slightly different than model 2 as high temperature region can be seen in the middle of crown in model 1, but not in model 2.

4.2 Von MisesStress Distribution

The Von Misesstresses in the pistonfromthe thermo-mechanical analysis are given in Fig. 9 and 10 for models 1 and 2 respectively. The stresses were probed at two critical locations that cause thermo-mechanical fatigue failures in pistons [24-26]. These locations are the pin hole and the crown areas located on the same vertical plane that contains the pin hole (encircled in red in Fig. 9 and 10). As can be seen, the maximum Von Misesstress in the piston for both FE models occurred at the web and boss interface.
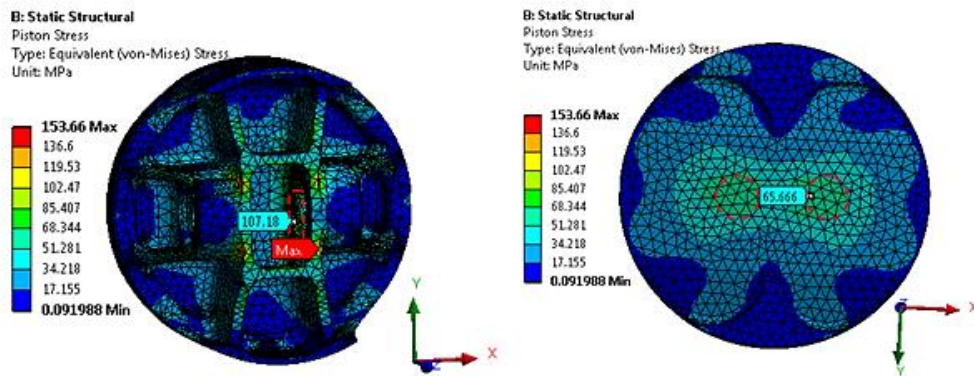
Figure 9. Critical stress areas in piston in model 1.
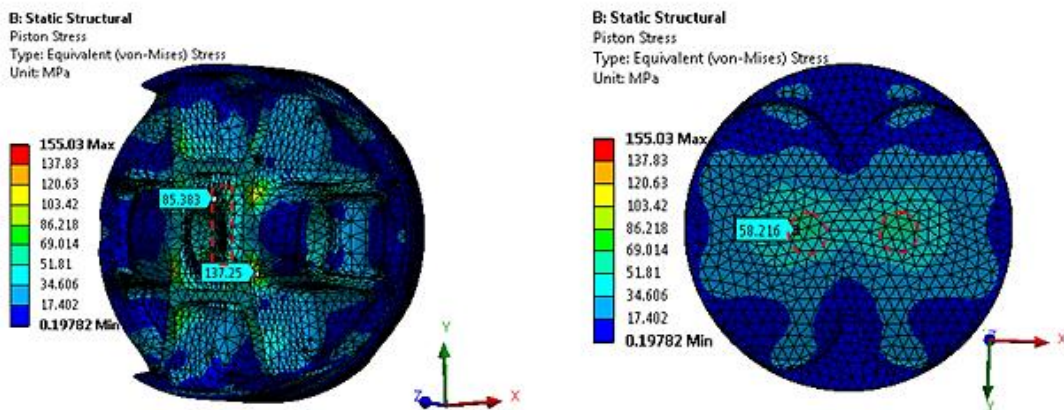
Figure 10. Critical stress areas in piston in model 2.

4.3 Strain Distribution
The elastic strains in the critical areas were also probed to see if they follow the same trends as the stresses. These are plotted in Fig. 11 and 12 for models 1 and 2 respectively.
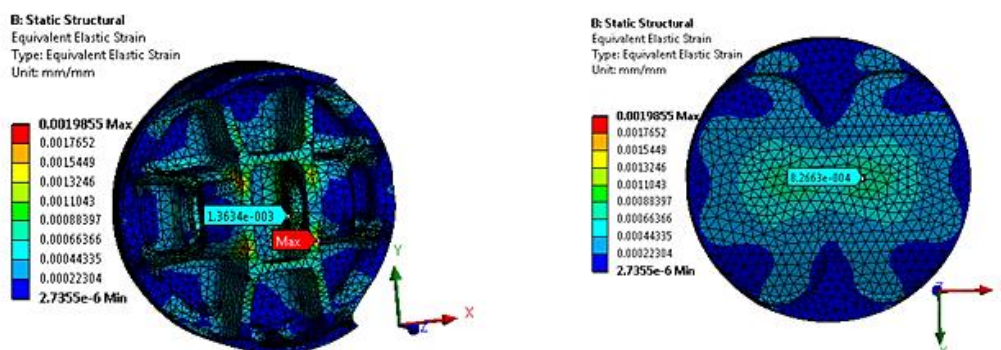
Figure 11. Piston elastic strains in critical stress areas in model 1.
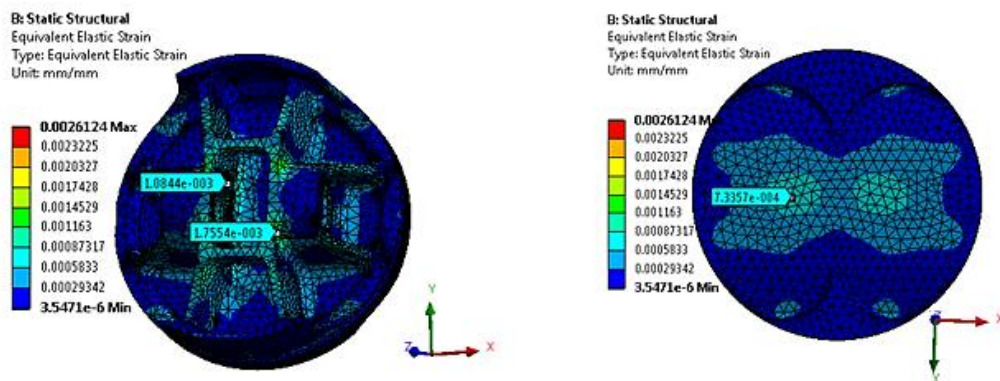
Figure 12. Piston elastic strains in critical stress areas in model 2.

As can be seen the maximum strains occurred at approximately the same locations as the maximum Von Mises stresses seen in section 4.2.

4.4 Maximum Principal Stress Distribution
        The majority of pistons produced are heat treated to the T6 condition which reduces the ductility from the as manufactured component. Reduced ductility combined with the stress concentrations at pin holeand web-boss interface may cause the piston to fail in brittle manner as

described by [26]. Brittle failure or fracture is associated with no visual ormacroscale plastic deformation ofa material [27]. It was therefore deemed important to investigate the maximum principal stresses in the pistons whichwere probed at the same locations as in section 4.2. The results of principal stressesare shown in Fig. 13 and 14for models 1 and 2 respectively. The stresses in model 1 were 19.4% and 12% higher in pin hole and crown locations respectively than model 2.
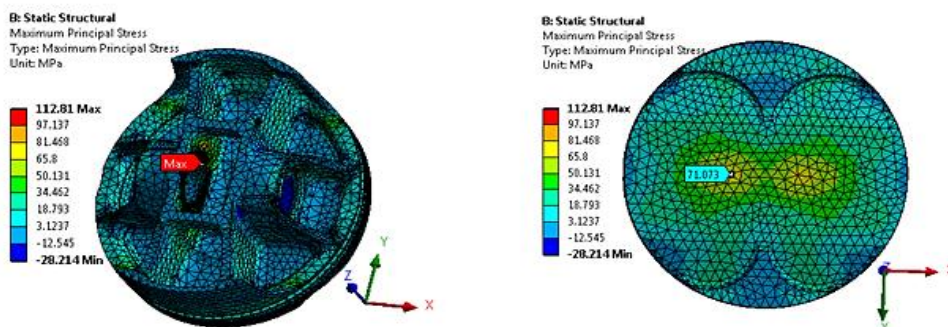
Figure 13. Maximum principal stresses in piston in model 1
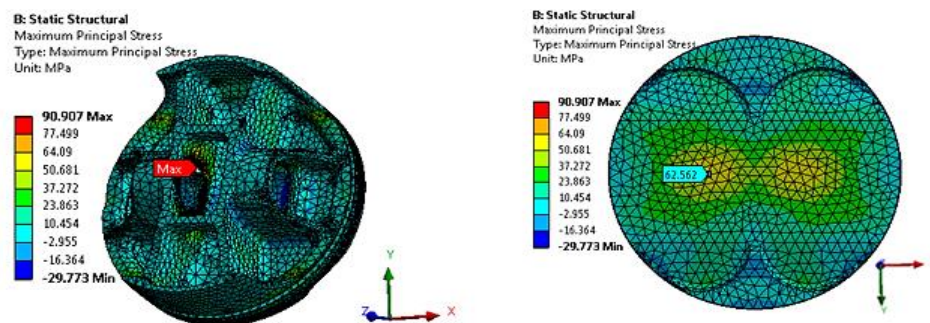
Figure 14. Maximum principal stresses in piston in model 2.

From the results it can be seen that model 1 is giving higher stresses than model 2 and would therefore be more conservative in terms of piston

design. Depending on how critical mass reduction is in terms of the engine design,model 1 or 2 might be selected based on stresses only. Stress though is

not the only criterion that needs to be considered when designing pistons. The deformation that the piston undergoes during engine operation governs the piston cold mounting clearance values and must also be taken into account. The results for the piston deformationsare given in section 4.5.

4.5 Piston Directional Deformations

The directional deformations of the piston are given in Fig. 15-20. All the piston directional deformations were taken relative to piston crown centre on the top surface. The dashed lines represent positions along which measurements have been made.

The piston deformations in the X directions for both models are shown in Fig. 15, measured along the dashed line shown in Fig. 16, with the respective piston displacement plotsshown in Fig. 16.
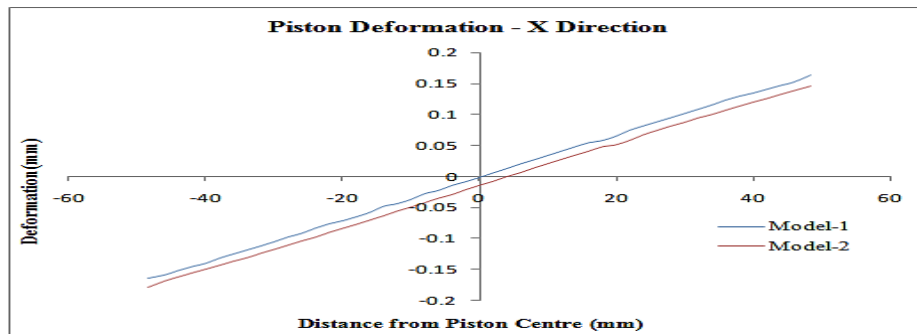
Figure 15. Piston deformation graphs in X directions for both FE models.
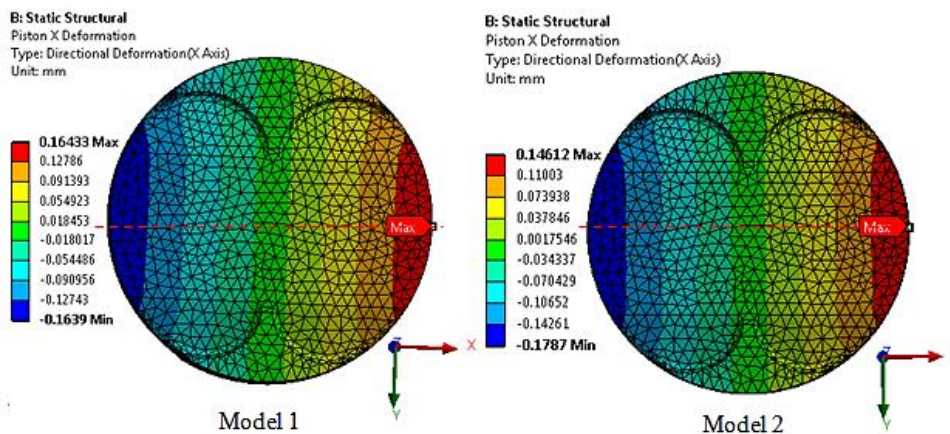
Figure 16. Piston deformation plots in X directions for both FE models.

The piston deformations in the Y directions for both models are shown in Fig. 17, measured along the dashed line shown in Fig. 18, with the respective piston displacement plotsshown in Fig. 18.
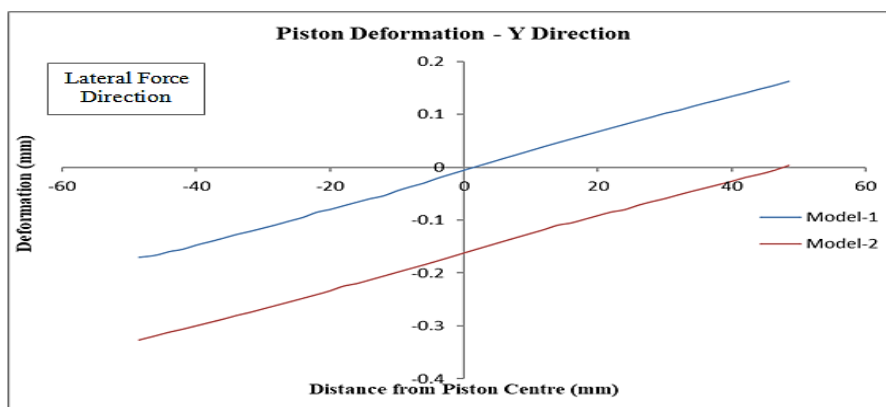
Figure 17. Piston deformation graphs in Y directions for both FE models.
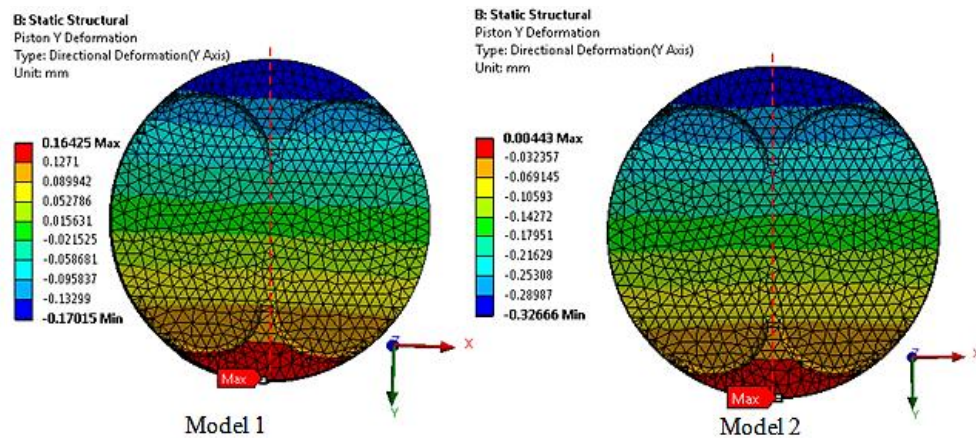
Figure 18. Piston deformation plots in Y directions for both FE models.

The piston deformations in the Z directions for both models are shown in Fig. 19, measured along the dashed line shown in Fig. 20, with the respective piston displacement plots shown in Fig. 20.
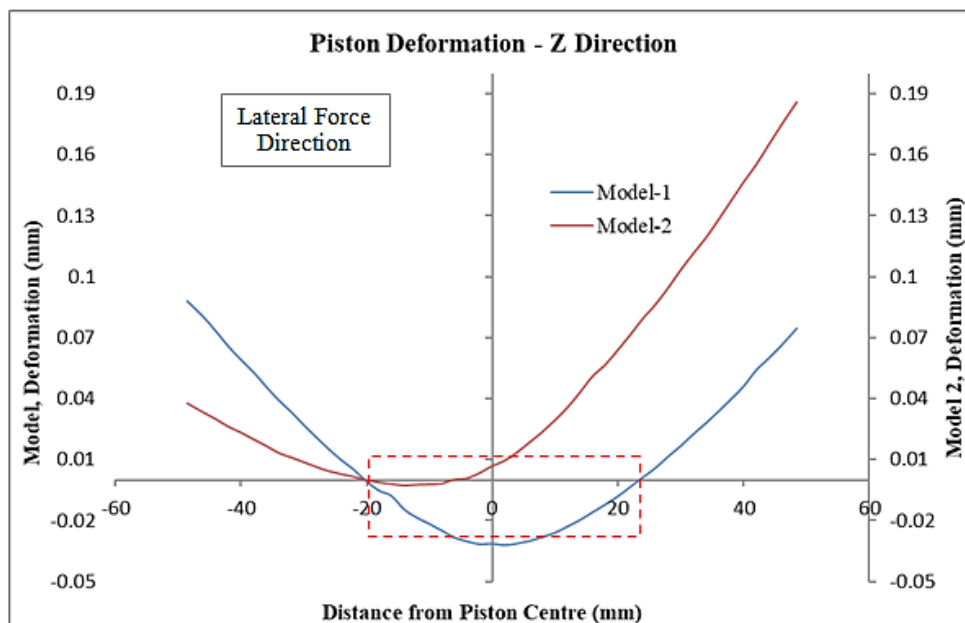
Figure 19. Piston deformation graphs in Z directions for both FE models.
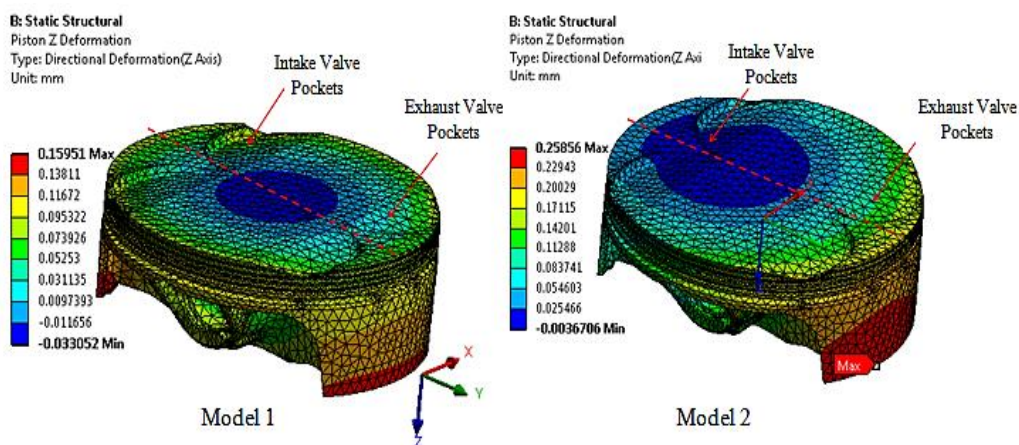
Figure 20. Piston deformation plots in Z directions for both FE models.

Fig. 21 shows the pin deformations looking along the Y axis for the two different models. The pin in model 1 shows a dome shaped deformation, while the pin in model 2 is compressed by the connecting rod in the middle.
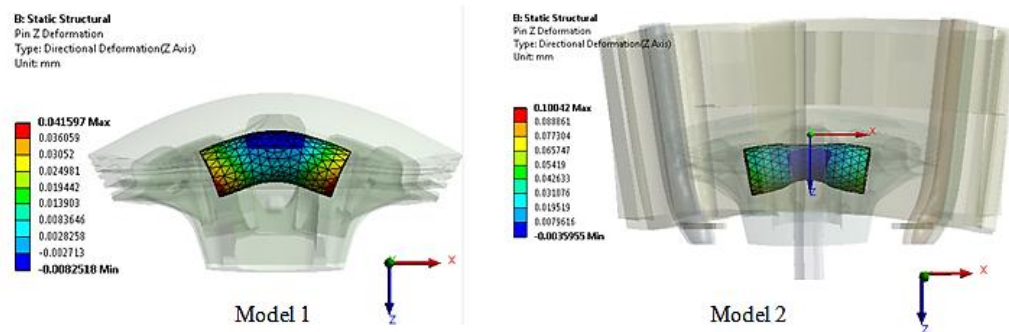
Figure 21. Pin deformation plots in Z direction in both FE models.

V.   DISCUSSION

The quasi-static temperature distribution in the pistons in Fig. 7 indicated thatthe maximum temperature was nearly the same in both FE models, however the temperature distribution in model 1 is slightly different than model 2 as high temperature region can be seen in the middle of crown in model 1, but not in model 2.The high temperature region was only 1degree higher than the immediate surrounding area on the crown. The lack of the high temperature region in the middle of crown in model 2 could be due to the cylinder (Fig. 8) absorbing some of the heat from the piston.

From the stress results in Fig. 9 and 10, it is clear that the different approaches are significant in terms of the difference in stresses produced. The stresses in the pin hole and the crown were higher in model 1. The stresses in model 1 were approximately 20.3 % and 11.3 % higher than model 2 at the pin-holeand onthe crown critical areas (see section 4.2)respectively. The lower stresses in model 2 is associated with the larger inertial force, generated by the higher mass of the moving components due to addition of the connecting rod and the fact that the inertial force generates opposing flexure to that of the combustion pressure effect [8].

Furthermore, the elastic strains in model 1 (Fig. 11) were approximately 20.5% and 11.3% higher than model 2 (Fig. 12) at the pin-hole and crown critical areas respectively. The percentage differences between the Von Misesstresses and strains are nearly the same for both FE models at the crown whilst slightly different for the pin-hole locations. The elastic strains seem to be following the stress trends in both FE models. In addition, the maximum principal stresses in model 1 (Fig. 13) were 19.4% and 12% higher in the pin hole and the crown critical areas respectively than in model 2 (Fig. 14).

Piston deformations in the X and Y directions affect the piston to cylinder running clearances which in turn might affect the engine performance. Larger piston-cylinder clearances lead to compression loss while smaller piston-cylinder clearances increase friction between piston and cylinder. Both of these conditions are likely to reduce engine performance. Improper piston-cylinder clearances also reduce piston fatigue life and can cause engine seizure [28].

The piston deformations in the X directions for both models were nearly the same as can be seen in the graph in Fig. 15 and their respective deformation plots as shown in Fig. 16. The equal deformations in the X directions were due to the same loading conditions on both side of the piston crown centre in the X directions.

The piston deformations in the Y directions in Fig. 17 and 18 indicatethat the piston in model 2 moved in the negative Y direction due to the lateral force. The movement in the negative Y direction will generate compressive stresses due to the piston being pressed against the cylinder wall. Since the piston deformations in the Y direction are approximately symmetrical in model 1 (Fig. 17 and 18), it indicates that the lateral force was not fully transferred to the piston due to the pin-connecting rod interface constraint.

The piston deformations in the Z directions in Fig. 19 and 20 suggested that the piston in model 2 deformed approximately 2.5 times more on one side (opposite to the lateral force) compared to model 1. This is because the lateral force presses the piston against the cylinder resulting in increased friction between the piston and cylinder, hindering the piston deformation in the Z direction, caused by the combustion pressure. On the other side of the pistonthere is reduced frictionallowingmore of the effect of the combustion pressure to be realised which increases the Z direction deformation.

The piston deformations in the Z directions suggested that the piston crown in model 1 deformed much more in the negative Z direction

then in model 2 (shown in red dashed lines in Fig. 19). Piston deformation in the Z direction affects the clearances between piston crown, intake and exhaust valves. The higher deformations in negative Z direction in model 1 may cause the piston designer to allowlarger piston-valve clearances than necessary which will impact the compression ratio leading to reduced engine performance.

The piston-valve clearances have tighttolerances and in the case of the engine looked at in this work the cold piston-valve clearance ranges are 0.07 – 0.13mm for intake and 0.12 – 0.18 mm for exhaust valves respectively. The larger clearances required on the exhaust valves are due to the exhaust valves expanding more than the intake valves. The deformations of the intake and exhaust valve pockets in both models were probed to determine the valve pocket deformations that will suggest the least piston to valve clearances (more likely to make contact with the valves).The higher deformation of the valve pockets in the negative Z direction or lower deformation in positive Z direction will dictate piston to valve clearances. The deformations of the intake valve pockets were – 0.007 and – 0.002mm, while for the exhaust valve pockets the values were 0.009 and 0.084 mm for models 1 and 2 respectively.

The results indicated that the exhaust valve pockets deformed more than the intake valve pockets in both FE models, which is realistic. However, the larger deformation of intake valve pockets in the negative Z direction and the smaller deformation of the exhaust valve pockets in the positive Z direction in model 1 indicate that model 1 will predict smaller piston to valve clearances than model 2. Based on the valve pockets deformations, model 1 is suggesting 3.5 and 9.1 times lower piston to valve clearances than model 2 for intake and exhaust valve pockets respectively. This could lead to allowing larger piston-valve clearances than needed (affecting piston compression height), to avoid piston hitting the valves, which will affect the compression ratio and may reduce engine performance.

The anti-thrust side (opposite to the lateral force direction side or exhaust valve pocket side) of the piston skirt is made thicker in designs to resist the larger deformation as described above (model 2 in Fig. 20). These deformation differences cannot be seen in model 1 and would therefore lead to flawed skirt design. The skirt thicknesses in thrust and anti-thrust sides for the piston investigated in this work are 2.255 mm and 2.505 mm respectively. The strength of the skirt maintains the piston axis parallel to the cylinder axis and is the major controlling factor at operating temperatures

affecting ring land size and outside diameter, and the ring attitude normal to the cylinder face [29].

The unrealistic piston deformations in the Z direction in model 1 may have been caused by the unrealistic pin deformation. As the ends of the pin bend in the positive Z direction (bowed down) due to the combustion load, the middle of the pin bends in the negative Z direction (see displacement plots in Fig. 21) due to the pin-connecting rod constraint. Since the piston was supported by the pin; the piston followed the same deformation pattern which may have led to improper piston deformations in the Z direction at the middle of the crown. The pin deformation plots in Fig. 21 showed that the pin in model 2 was compressed in the middle by the connecting rod, which seems more realistic.

VI. CONCLUSION
The work undertaken in this paper analysed two different approaches as suggested in literature forthe FEA modelling of a piston.The work highlights the importance of accounting forthe lateral forces in piston FEAs, which are largely ignored in most publications.The results shows that using piston, pin, some portion of the connecting rod and a cylinder (model 2) is a more realistic representation of the structural response of the piston assembly compared to the combination of only piston and pin (model 1) that is widely used in literature.The work highlights that,model 1 may overestimate the stresses and produce unrealistic deformations in the piston which may lead to an improper design.Model 2 leads to more realistic pin deformation and allows the action of the lateral force on the piston to be incorporated. The deformations so obtained have significant effect on possible piston clearances and skirt design choices.The results demonstrate the significance of making appropriate model choices in order to obtain realistic results for piston design.

REFERENCES
[1]. Xu T, Hwang SJ, Tang CY, Ejakov M, King M. An advanced and comprehensive CAE approach of piston dynamics studies for piston optimal and robust design. SAE International Journal of Engines. 2011 Jan 1;4(1):2087-99.
[2]. Cha SW, Ha EJ, Lee KW, Chang H. Development of fatigue durability analysis techniques for engine piston using CAE. SAE International Journal of Materials and Manufacturing. 2009 Jan 1;2(1):403-8.
[3]. MAHLE GmbH. Engine testing. Pistons and engine testing. 2016:115-280.
[4]. Carvalheira P, Gonçalves P. Fea of two engine pistons made of aluminium cast alloy A390 and ductile iron 65-45-12 under service conditions. In5th International Conference on Mechanics and

Materials in Design Porto-Portugal 2006 (pp. 24-26).

[5]. Okamoto H, Anno N, Itoh T. New Computational and Experimental Stress Analysis Method for the Design Decision on Optimum Piston Configuration of Production Engine. SAE Technical Paper; 1992 Feb 1.

[6]. Singh L, Rawat SS, Hasan T, Kumar U. Finite Element Analysis of Piston In ANSYS. International Journal of Modern Trends in Engineering and Research (IJMTER) Volume. 2015;2.

[7]. Norton RL. Design of machinery: an introduction to the synthesis and analysis of mechanisms and machines. Boston: McGraw-Hill; 1999.

[8]. Wang YX, Liu YQ, Shi HY. Finite Element Static and Dynamic Analysis for a Piston. InAdvanced Materials Research 2010 (Vol. 97, pp. 3323-3326). Trans Tech Publications.

[9]. Schneider C, Halbhuber J, Wachtmeister G. Measuring and Simulating Friction between Piston Pin and Connecting Rod on a Tribometer Test Bench to Define Locally Resolved Friction Coefficients. SAE Technical Paper; 2016 Apr 5.

[10]. Aluminium Federation. The properties of aluminium and its alloys. Birmingham: Aluminium Federation; 1993.

[11]. Handbook M. Properties and selection: nonferrous alloys and pure metals. American Society for Metals, Metals Park, OH. 1979.

[12]. Sheppard B. Engineering student and formula student team member at Oxford Brookes University. Personal Communication. 25th January 2017.

[13]. Munyao E, He J, Zhiyuan Y, Yi Z. Simulation of Thermal-Mechanical Strength for Marine Engine Piston Using FEA. Journal of Engineering Research and Applications. 2014;4(3):319-23.

[14]. Hamzehei M, Rashidi M. Determination of piston and cylinder head temperature distribution in a 4-cylinder gasoline engine at actual process. InProceedings of the 4th WSEAS Int. Conf. on heat transfer, thermal engineering and environment, Elounda, Greece 2006 Aug 21.

[15]. Hohenberg GF. Advanced approaches for heat transfer calculations. SAE Technical paper; 1979 Feb 1.

[16]. Pulkrabek WW. Engineering fundamentals of the internal combustion engine. 2nd Ed. Essex: Pearson; 2014.

[17]. Woschni G. A universally applicable equation for the instantaneous heat transfer coefficient in the internal combustion engine. SAE Technical paper; 1967 Feb 1.

[18]. Torregrosa AJ, Olmeda PC, Romero CA. Revising engine heat transfer. Journal of Engineering Annals of Faculty of Engineering Hunedoara. 2008;6(3):245-65.

[19]. Sanli A, Ozsezen AN, Kilicaslan I, Canakci M. The influence of engine speed and load on the heat transfer between gases and in-cylinder walls at fired and motored conditions of an IDI diesel engine. Applied thermal engineering. 2008 Aug 1;28(11-12):1395-404.

[20]. Mizuno H, Ashida K, Teraji A, Ushijima K, Takemura S. Transient analysis of the piston temperature with consideration of in-cylinder phenomena using engine measurement and heat transfer simulation coupled with three-dimensional combustion simulation. SAE International Journal of Engines. 2009 Jan 1;2(1):83-90.

[21]. Ezzulddinyousif I, Al-Quraishi BM, Al-Beiruti AA. Thermal effects on diesel engine piston and piston compression rings. Engineering and Technology Journal. 2009;27(8):1444-54.

[22]. Turner M. Part Department Manager at Premier Bikes, Didcot, UK. Personal Communication. 4thth January 2019.

[23]. Esfahanian V, Javaheri A, Ghaffarpour M. Thermal analysis of an SI engine piston using different combustion boundary condition treatments. Applied Thermal Engineering. 2006 Feb 1;26(2-3):277-87.

[24]. Dileep M, Sanjay PS, Mandloi RK. Analytical study of fatigue failure of aluminium alloy piston in IC engines. Inter Res Jour of Eng and Tech. 2016;3:1665-9.

[25]. Silva FS. Fatigue on engine pistons–A compendium of case studies. Engineering failure analysis. 2006 Apr 1;13(3):480-92.

[26]. Floweday G, Petrov S, Tait RB, Press J. Thermo-mechanical fatigue damage and failure of modern high performance diesel pistons. Engineering Failure Analysis. 2011 Oct 1;18(7):1664-74.

[27]. Becker WT. Ductile and Brittle Fracture.

[28]. Bonelli M, Garzon G, Marino D, Audebert F, Errazquin J. EVALUACIÓN DE LA PERFORMANCE DE PISTONES DE COMPETICIÓN ELABORADOS CON NUEVAS ALEACIONES DE ALUMINIO. Argentina. University of Buenos Aires. 2014.

[29]. Azevedo MN, ChiquitoFilho S. Lightweight Pistons. SAE Technical Paper; 1988 Feb 1.